Proceedings of the 10th Brazilian Congress of Thermal Sciences and Engineering -- ENCIT 2004
Braz. Soc. of Mechanical Sciences and Engineering -- ABCM, Rio de Janeiro, Brazil, Nov. 29 -- Dec. 03, 2004

Paper CIT04-0341

VISCOELASTIC FLOW IN AXISYMMETRIC CONTRACTIONS: THE EFFECT OF CONTRACTION RATIO

Manuel António Alves
Departamento de Engenharia Química, CEFT, Faculdade de Engenharia da Universidade do Porto, 4200-465 Porto, Portugal
mmalves@fe.up.pt

Fernando Tavares de Pinho
Centro de Estudos de Fenómenos de Transporte, Dep. Eng. Mecânica, Universidade do Minho, 4800-058 Guimarães, Portugal
fpinho@dem.uminho.pt

Paulo Jorge Oliveira
Dep. Eng. Electromecânica, Unidade de Materiais Têxteis e Papeleiros, Universidade da Beira Interior, 6201-001 Covilhã, Portugal
pjpo@ubi.pt

Abstract. *Numerical simulations of PTT fluids in axisymmetric sudden contractions were carried out to investigate the effect of contraction ratio on the flow patterns under conditions of negligible inertia. The PTT model selected has a linear stress coefficient, and contraction ratios (CR) in the range 4:1 to 100:1 were investigated. The simulations are based on a finite volume methodology using very fine meshes and a purposely developed high-resolution scheme for the discretization of advective terms in the viscoelastic constitutive equation. In contrast to Newtonian fluids, where the contraction ratio has no significant influence for CR larger than 4, for these shear-thinning viscoelastic fluids the corner vortex increases with flow elasticity and, of more interest, a lip vortex is formed at large contractions ratios. This lip vortex also grows with elasticity, then merges and later engulfs the corner vortex, much like the situation for plane contraction flows. In this work, maps are presented outlining regions of different vortex behaviour.*

Keywords*. Viscoelastic flow, computational rheology, circular contraction, effect of contraction ratio, PTT model.*

1. Introduction

Benchmark flow problems in computational rheology are still very important, because they can provide very accurate results for code validation, while still highlighting new features in flows which have been simulated only over a limited range of relevant conditions.

The flow of viscoelastic fluids in a sudden contraction was suggested as a benchmark problem in 1987, during the 5th International Workshop on Numerical Methods in Non-Newtonian Flows (Hassager, 1988), for the specific contraction ratio of 4:1 (ratio between the radius of upstream and downstream tubes – see Fig. (1) for flow configuration and main notation). Since 1988 there has been considerable interest on the numerical simulation of this benchmark flow, and most of the works were based on the specified 4:1 planar contraction (e.g., Yoo and Na, 1991; Sato and Richardson, 1994; Matallah et al, 1998; Oliveira and Pinho, 1999; Phillips and Williams, 1999; Alves et al, 2000; Al Moatassime et al, 2001; Aboubacar et al, 2002; Meng et al, 2002; Alves et al, 2003b), or the 4:1 circular contraction case (e.g. Coates et al, 1992; Sasmal, 1995; Baaijens, 1998; Wachs and Clermont, 2000; Phillips and Williams, 2002; Alves et al, 2003c). In terms of experimental studies there is also a large number of works for both planar and circular contractions, and the effect of the contraction ratio was analyzed in some of them (e.g. Evans and Walters, 1986; Rothstein and McKinley 2001; Nigen and Walters, 2002). For a detailed review of the main experimental and numerical studies on planar and axisymmetric contractions the interested reader is referred to the recent book of Owens and Phillips (2002).

Despite this large body of works it has been recognized later (Nigen and Walters, 2002) that this specific 4:1 ratio was not probably the best choice, as many interesting features of an actual contraction flow are not emphasized. These authors suggested that flows in contractions having ratios other than the standard 4:1 value should be explored in more detail. A survey of the literature reveals only a few studies, mainly experimental, where the variation of contraction ratio is considered. Hence, while the existing numerical data for the 4:1 contraction may remain as a valid benchmark data set for assessment of newly developed simulation codes, there is also a need for a systematic investigation of the role of contraction ratio on viscoelastic flow through contractions. We have recently undertaken this task for planar contractions (Alves et al, 2004), and now we aim to explore the same effect in circular contractions.

2. Governing equations

The flow of an incompressible viscoelastic fluid is described by the continuity and momentum equations,

$$\nabla \cdot \boldsymbol{u} = 0 \tag{1}$$

$$\rho\left[\frac{\partial \boldsymbol{u}}{\partial t}+\nabla\cdot(\boldsymbol{uu})\right]=-\nabla p+\eta_s\nabla\cdot\left(\nabla\boldsymbol{u}+\nabla\boldsymbol{u}^{\mathrm{T}}\right)+\nabla\cdot\boldsymbol{\tau} \tag{2}$$

coupled with an appropriate constitutive equation for the extra stress tensor, $\boldsymbol{\tau}$. In this work the simplified version of the Phan-Thien—Tanner model (PTT) was selected, which is expressed as (Phan-Thien and Tanner, 1977)

$$\lambda\left[\frac{\partial \boldsymbol{\tau}}{\partial t}+\nabla\cdot(\boldsymbol{u\tau})\right]+f(\boldsymbol{\tau})\ \boldsymbol{\tau}=\eta_p(\nabla\boldsymbol{u}+\nabla\boldsymbol{u}^{\mathrm{T}})+\lambda(\boldsymbol{\tau}\cdot\nabla\boldsymbol{u}+\nabla\boldsymbol{u}^{\mathrm{T}}\cdot\boldsymbol{\tau}) , \tag{3}$$

where the stress coefficient function, $f(\boldsymbol{\tau})$, depends on the trace of the extra stress tensor. Following Phan-Thien and Tanner (1977), the linear version of $f(\boldsymbol{\tau})$ was selected,

$$f(\boldsymbol{\tau})=1+\frac{\lambda\varepsilon}{\eta_p}\mathrm{Tr}(\boldsymbol{\tau}) , \tag{4}$$

where λ represents the relaxation time of the fluid, ε is an extensional-related parameter of the model and η_p is a polymer-related viscosity coefficient, as opposed to the solvent viscosity η_s in Eq. (2). The sum of the two viscosities is $\eta_0=\eta_p+\eta_s$, and represents the zero-shear-rate viscosity of the fluid in a simple shear flow. In the PTT model the polymer viscosity is shear thinning, and the parameter η_p represents its zero-shear-rate value. A solvent viscosity ratio $\beta=\eta_s/\eta_0$ is used to prescribe the amount of η_s in comparison to η_p .

3. Numerical method

The equations presented on the previous section are initially transformed into a general non-orthogonal co-ordinate system, for easy application of the finite-volume method (FVM) in a collocated mesh arrangement. Then, the equations are integrated over the set of control volumes (cells) and discretised. The dependent variables to solve for are the Cartesian components of the velocity vector and the polymer stress tensor, and pressure, all stored at the centre of the cells. Although in this work we are only interested in steady-state solutions, the time-dependent terms presented in Eqs. (2) and (3) are retained in the discretization, so that the steady-state solution is approached by a successive time-advancement of the solution. At each time step fully-implicit sets of algebraic equations need to be solved for each dependent variable, and preconditioned conjugate gradient methods are used for that purpose.

The first equations to be solved are those for the extra stress tensor components (Eq. 3), which are solved sequentially for each component, by assuming the velocity field from the previous time step. Then, the momentum equations (Eq. 2) are solved sequentially for each Cartesian velocity component, with the previous pressure field and the newly calculated stress fields. Finally, the discretised form the equation of mass conservation (Eq. 1) that was re-arranged into a Poisson pressure-correction equation, is solved implicitly for the pressure correction, p' . This correction is then added to the pressure field calculated in the previous time step, and is also used to calculate the velocity corrections in order to provide a new divergence-free velocity field. These steps are repeated until the norm of the residuals of all equations becomes smaller than a prescribed convergence tolerance. Typically, a normalized sum of residuals of order of 10^{-4} is used; it has been checked from numerical experiments that this tolerance, in terms of normalized variables, provides an adequately converged solution. A detailed description of the numerical method can be found in Oliveira et al (1998) and on the subsequent works: Oliveira and Pinho (1999), Oliveira (2001) and Alves et al (2000; 2003a).

The diffusive terms of the momentum equations are discretised with second-order central differences (CDS). The convective term in the momentum equation, although presented in Eq. (2), was neglected in this work, since we are concerned with creeping flow conditions (*Re*=0). On the other hand, the discretization of the convective term in the constitutive equation is very important due to its hyperbolic nature. In previous works we have implemented classical high-resolution schemes, such as MINMOD and SMART (Alves et al, 2000; 2001). Although bounded, we found that these classical high-resolution schemes could lead to a significant slowdown in the convergence rate and, in certain problems, even to an impossibility of attaining adequate fully iterative convergence. To circumvent this limitation of classical high-resolution schemes, in Alves et al (2003a) a new scheme was proposed, named CUBISTA. There, it was demonstrated that CUBISTA possesses enhanced iterative convergence properties, especially suitable for viscoelastic calculations (Alves et al 2003a,b), and consequently in this work the discretization of the advective term in the constitutive equation is done with this scheme, which is formally third-order accurate.

4. Problem definition and computational meshes

The flow geometry is illustrated in Fig. (1), where some of the relevant variables and features are also shown. The effect of contraction ratio (*CR*) will be studied in detail, which is here defined as,

$$CR = \frac{R_1}{R_2} \tag{5}$$

where R_1 represents the radius of the larger, incoming tube and R_2 the radius of the smaller, outflow tube. Other dimensionless groups characterizing this flow are the solvent viscosity ratio defined in Section 2, $\beta = \eta_s / \eta_0 = 1/9$, the extensional parameter of the PTT model, here taken as $\varepsilon = 0.25$, and the Deborah number defined in terms of downstream quantities,

$$De = \frac{\lambda U_2}{R_2} \tag{6}$$

where U_2 represents the average velocity in the outflow tube. Inertia could be measured by a Reynolds number but, for the creeping flow conditions considered here, this parameter plays no role and was set to zero, i.e. the advective term in Eq. 2, $\nabla \cdot \rho \boldsymbol{uu}$, was dropped.

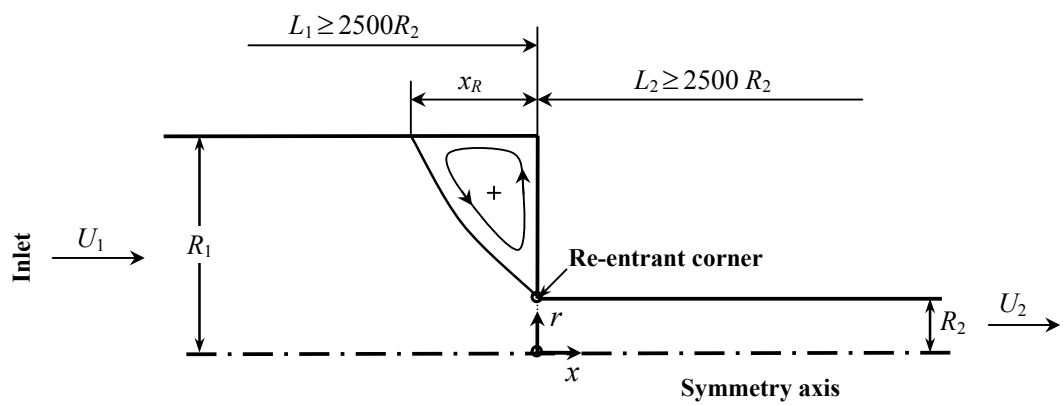

Figure 1. Schematic of the flow configuration.

The basic information about the computational meshes is presented in Table 1, which includes the lengths of the upstream and downstream tubes (L_1 and L_2), the total number of cells (*NC*), the number of degrees of freedom (*DOF*), and the size of the smallest cell near the re-entrant corner ($\Delta x_{\min}$, $\Delta y_{\min}$, both normalized with R_2). The meshes used in the simulations are non-uniform with a larger concentration of cells in the vicinity of the problematic re-entrant corner and along the tube walls, where the velocity and stress gradients are expected to be large. It is quite clear that the channel lengths L_1 and L_2 need to be varied according to the contraction ratio (and also *De*) so that adequate dimensions are provided for flow development and redevelopment upstream and downstream of the contraction plane. Increasing the *De* number leads to larger upstream and downstream tubes, in order to fully development of velocity and stress profiles. This point was demonstrated quantitatively in Alves et al (2003b), where appropriate correlations for L_2 were presented. To avoid the use of meshes with different lengths for varying *De* values, for a given contraction ratio, we chose the use of very large computational meshes, one for each *CR* value, as shown in Tab. (1).

An illustrative example of the computational meshes used is given in Fig. (2) for *CR*=100. Only a zoomed region near the contraction plane is shown to illustrate the high degree of refinement near the re-entrant corner and the walls. An important aspect is that the mesh dimensions near the re-entrant corner are the same for all meshes (with a minimum cell spacing of $0.02R_2$) so that the local variations of the resulting solution fields are not influenced by the contraction ratio.

Table 1 – Main characteristics of the computational meshes

CR	L_1/R_2	L_2/R_2	*NC*	*DOF*	$\Delta x_{\min}=\Delta y_{\min}$
4	2 500	2 500	8 980	53 880	0.020
10	2 500	2 500	10 420	62 520	0.020
20	2 500	2 500	11 956	71 736	0.020
40	2 500	2 500	15 796	94 776	0.020
100	5 000	5 000	23 920	143 520	0.020

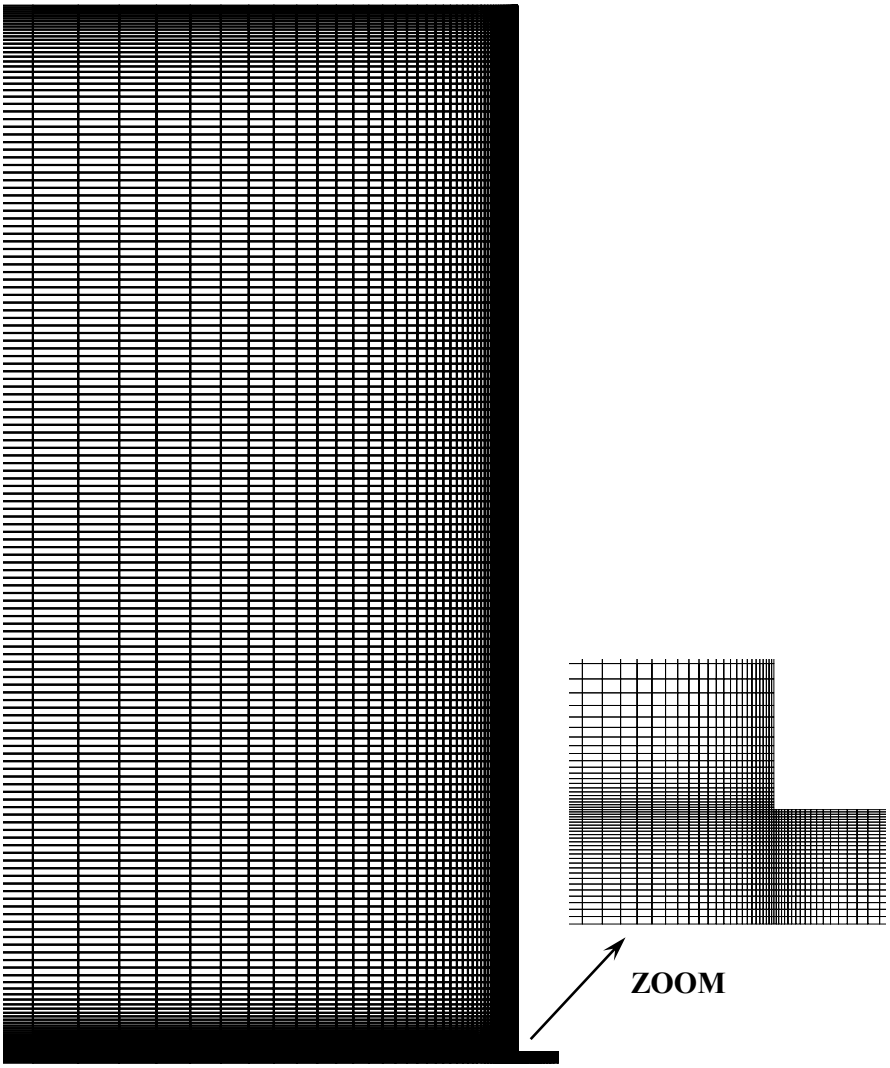

Figure 2. Zoomed view of the computational mesh used for *CR*=100.

5. Results and discussion

Firstly, in Section 5.1, streamline plots for different contraction ratios are presented as a function of the Deborah number. Based on these plots vortex maps are presented, which identify different types of vortices as a function of *CR* and *De* (or *De*/*CR*, as appropriate). Finally, in Section 5.2, scaling laws are presented and discussed for both vortex length and intensity.

5.1. Flow patterns

Even for creeping flow conditions, it is well known that different types of vortices can arise for viscoelastic flows in contractions, either planar or circular. For planar contractions, Alves et al (2004) demonstrated that the contraction ratio can have a marked influence on the vortex types for a PTT model; using the same parameters for the constitutive equation, we now aim to investigate the effect of the contraction ratio on the flow patterns in circular contractions.

Streamline contour plots are presented in Figs. (3) and (4) for *CR*= 4 and 100, respectively. Different vortex behaviours can be identified for increasing values of the Deborah number: whereas for the 4:1 circular contraction an intense vortex enhancement is observed, for the 100:1 contraction a more complex flow pattern is predicted, with the appearance of a small lip vortex at *De* values around 0.1-0.2, followed by an intense enhancement of this lip vortex, which engulfs the corner vortex at around *De*=10-20, creating a large lip vortex that continues to grow with increasing elasticity of the flow.

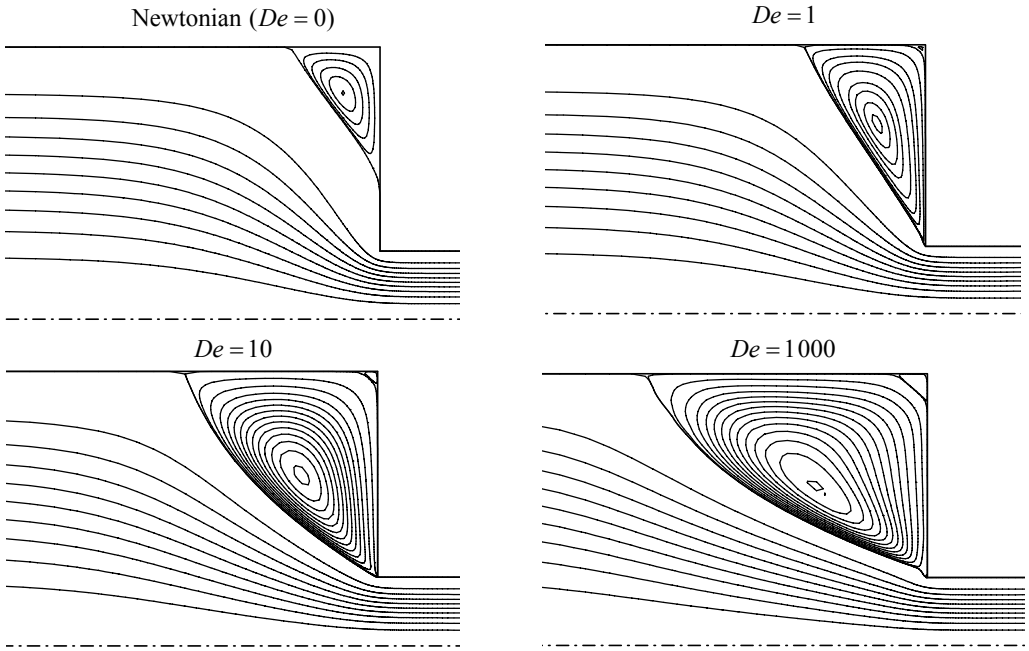

Figure 3. Streamline patterns for the 4:1 circular contraction.

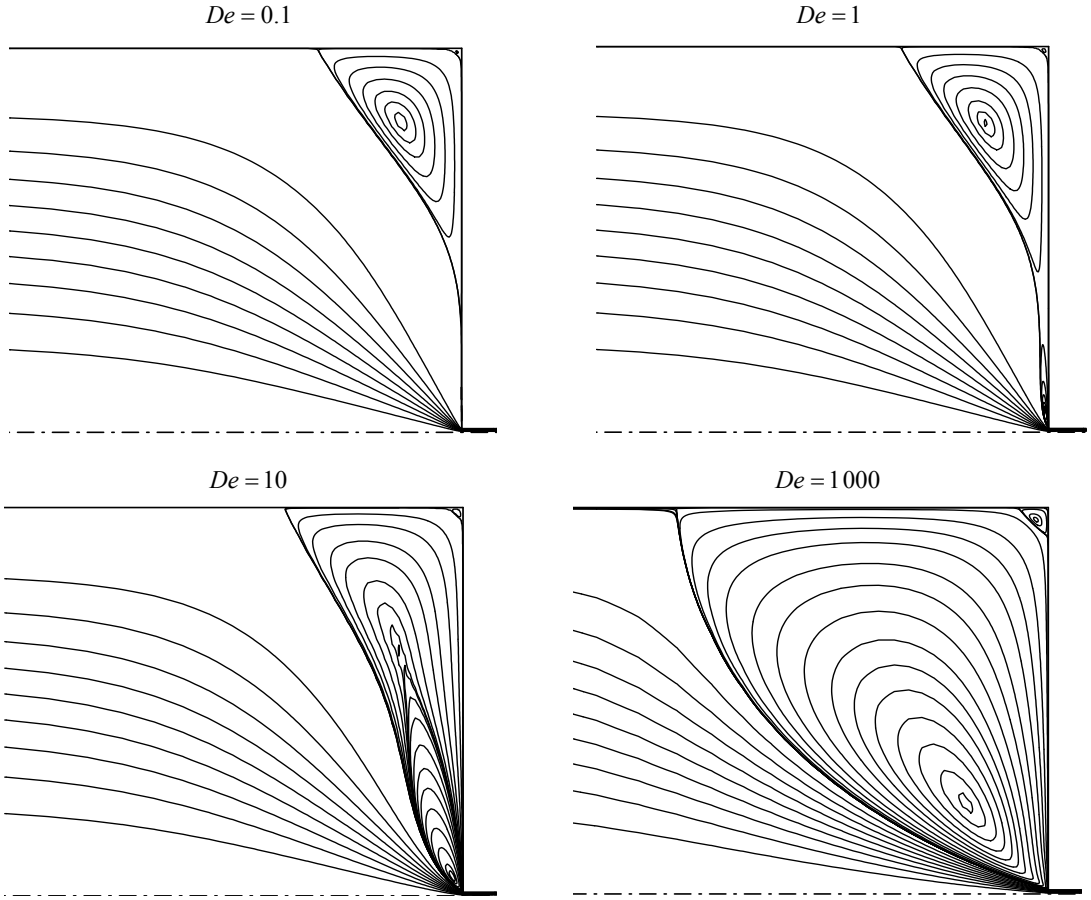

Figure 4. Streamline patterns for the 100:1 circular contraction.

With a view to classifying the structure of flows through circular contractions, we have carried out an extensive simulation program, for various contraction ratios and increasing Deborah numbers. The resulting flow patterns were classified as corner vortex, lip vortex, or as a combination of lip plus corner vortex structures. In Fig. (5) the outcome of this classification is plotted as a map of vortex type versus contraction ratio and Deborah number, or *De*/*CR*, in the same way as we did for planar contractions (Alves et al, 2004). The resulting vortex map is similar to the previous one obtained with planar contractions, and demonstrates once again that lip vortex formation is controlled by *De* (see the vertical dividing line in Fig. (5a)), while the onset of a single merged vortex is controlled by *De*/*CR* (vertical line on the right side of Fig. (5b)). The intense "vortex enhancement" correlates well with the final stages of the co-existence of corner and lip vortices, when the latter starts to dominante, and it is seen from Fig. (5b) to occur at around $De/CR \approx 0.1-0.2$. On the other hand, the formation of a lip vortex appears to occur at a fixed Deborah number for all contraction ratios above 20, and for the present constitutive model Fig. (5a) suggests a value of about $De \approx 0.1-0.2$. For the lower contraction ratios, $CR=4$ and 10, Fig. (5) shows no sign of appearance of a lip vortex, in agreement with the predictions for the planar contractions. Additional work is required to better fill the vortex maps of Fig. (5) for the PTT fluid, and especially to account for the effect of the model parameters β and ε, but the main features are well captured by the present results.

The main difference between the present results for circular contractions and the previous work for the planar case (Alves et al, 2004) is simply the reduction, by an order of magnitude, of the two critical numbers: the minimum *De* value for which the lip vortex first appears (around 0.1-0.2 in the present case, in contrast to $De \approx 1-2$ for the planar case), and the value of *De*/*CR* when the complete merging of the vortices occur (around 0.1-0.2 in the present case, in contrast to $De/CR \approx 1-2$ for the planar case).

5.2. Scaling laws for vortex size and intensity

Figure (6a) presents the results obtained for the corner vortex length as a function of the Deborah number and the contraction ratio, illustrating the strong influence of *CR* on the computed vortex length. However, if instead we plot x_R/R_1 (and not x_R/R_2) as a function of De/CR, see Fig. (6b), a good matching of the results is obtained for $CR \geq 20$.

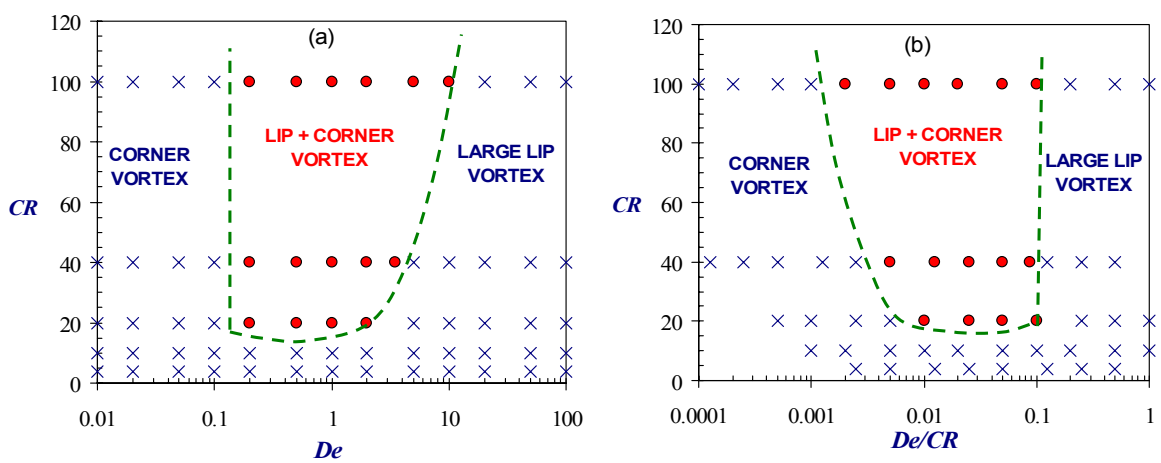

Figure 5. Vortex pattern maps: (a) Standard scaling; (b) Modified *De* scaling.

Figure (7) shows the variation of the salient corner vortex intensity (Ψ_R, a measure of the fluid entrapped in the secondary cell, defined by the recirculating flow rate in the corner vortex divided by the inlet flow rate into the contraction domain) with the modified Deborah number scaling, i.e. *De*/*CR*, for the various contraction ratios; in part (a) all data are plotted while in part (b) only data for $CR \geq 20$ are shown. Again, a reasonable correlation is achieved when Ψ_R is plotted versus *De*/*CR*, as occurred above with the vortex size. From the results in Fig. (7) one may conclude that *De*/*CR* is the proper scaling parameter for the corner vortex intensity, in the same way observed for planar contractions (cf. Alves et al, 2004).

For the intensity of the lip vortex, Ψ_{lip}, a different conclusion is reached, as shown in Fig. (8) where Ψ_{lip} is plotted as a function of *De*, for $CR \geq 20$. It should be pointed out that the lip vortex intensity is here taken as representing situations when a lip and a corner vortex coexist, or when the lip vortex merges with the corner vortex creating a large *lip vortex*. It is clear that the lip vortex, once formed, quickly grows with *De* to dominate the corner vortex and eventually completely engulfs that vortex to become the single remaining vortex structure (cf. Fig 4).

The fact that the lip vortex intensity scales with *De* is also apparent from the experimental data of McKinley et al (1991) for vortex size (cf. their Fig. 4), although it is not straightforward to reconcile those findings with our results because the data presented in McKinley et al (1991) refers to a Boger fluid flow in axisymmetric contractions at relatively low *CR* values.

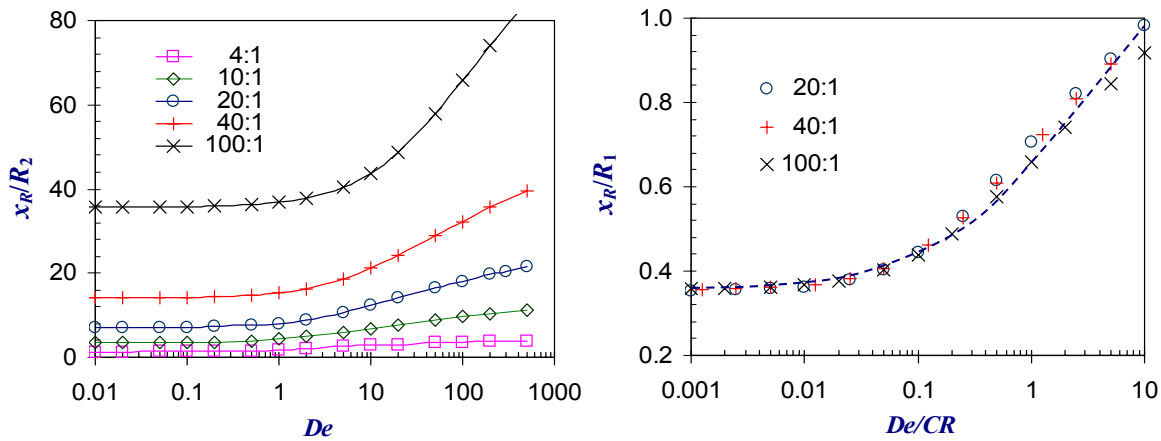

Figure 6. Variation of corner vortex size with Deborah number for different contraction ratios: (a) Standard scaling (all *CR*); (b) Modified scaling ($CR \geq 20$).

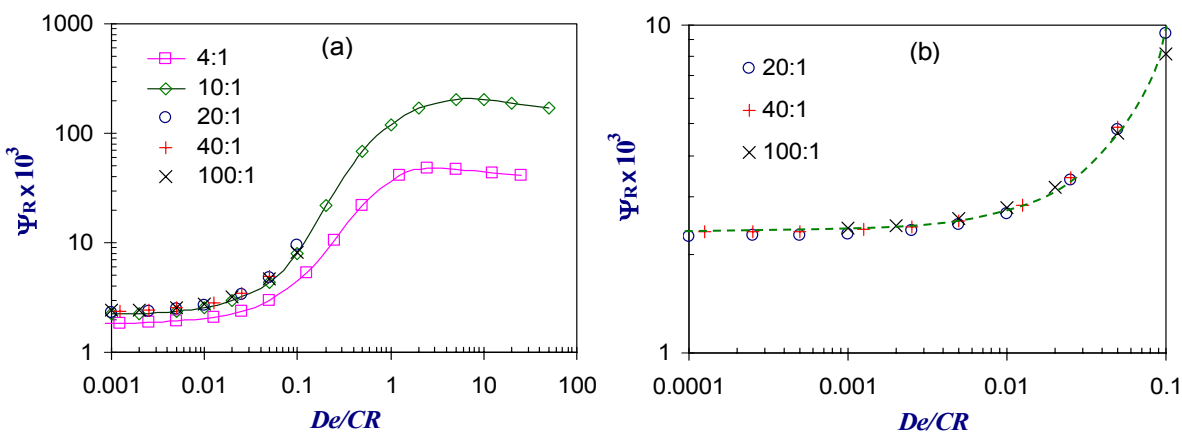

Figure 7. Variation of corner vortex intensity with the modified Deborah number, *De*/*CR*: (a) All *CR* values; (b) $CR \geq 20$.

Based on a large number of experimental results for Boger fluids in axisymmetric contractions, Rothstein and McKinley (2002) suggested a criterion to predict the transition from lip to corner vortex. These authors defined a dimensionless normal stress ratio as,

$$\mathcal{N} = \frac{N_1 / \eta_0 \dot{\gamma}}{(\tau_{zz} - \tau_{rr}) / \eta_0 \dot{\varepsilon}} = \frac{Sr(\dot{\gamma})}{Tr(\varepsilon)} \tag{7}$$

where *Tr* represents the Trouton ratio evaluated at the total Hencky strain accumulated along the centerline and $Sr(\dot{\gamma})$ represents the stress ratio. Rothstein and McKinley (2002) suggested that the characteristic shear-rate to consider in Eq. (7) should be taken as $\dot{\gamma} \approx \dot{\varepsilon} \approx U_2 / R_2$. Curiously, it turned out that the normal stress ratio was able to predict the onset of lip vortex for large *CR* values, as illustrated in Fig. (9) for different PTT parameter values (note that for $\varepsilon = 0$ the Oldroyd-B model is recovered, while for $\varepsilon = \eta_s = 0$ the Upper-Convected Maxwell model, UCM, is obtained). The hollow symbols in Fig. (9) represent flow conditions where a lip vortex is absent, while the filled symbols represent the cases where a lip and corner vortex coexist, or a large lip vortex dominates.

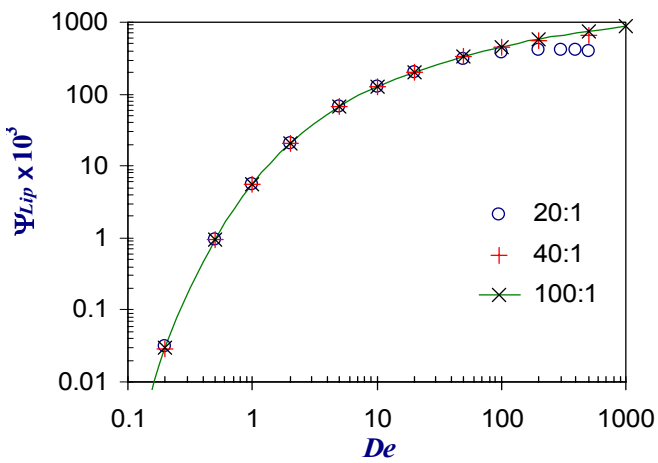

Figure 8. Variation of lip vortex intensity with Deborah number for different contraction ratios.

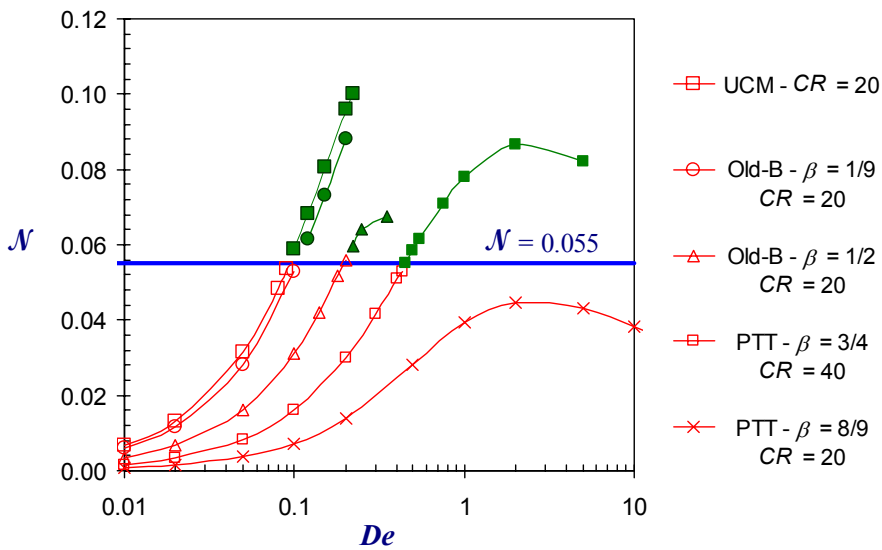

Figure 9. Influence of the normal stress ratio (defined in Eq. 7) on the vortex types.

6. Conclusions

Numerical simulations were carried out for creeping flow of a viscoelastic fluid through circular contractions of various contraction ratios. The results obtained complement our previous study with planar contractions (Alves et al, 2004), providing accurate numerical data for circular contractions with $CR = 4, 10, 20, 40$ and 100. The Phan-Thien/Tanner constitutive equation with a linear stress function was selected, with the parameters $\varepsilon = 0.25$ and $\beta = 1/9$. The results were rationalized in a vortex map, representing vortex types as a function of *CR* and *De* (or *CR* and *De*/*CR*), and a universal correlation of the data was obtained for $CR \geq 20$: the corner vortex intensity and the size, x_R / R_1, both correlate with *De*/*CR*, while the lip vortex intensity correlates with *De*. It was also found that for $CR \geq 20$ a lip vortex is formed at $De \approx 0.1 - 0.2$, which grows with elasticity and then engulfs the corner vortex at $De / CR \approx 0.1 - 0.2$. For $CR < 20$ it was found that increasing elasticity leads to a significant enhancement of the corner vortex size and intensity, without the appearance of any lip vortex.

The inception of a lip vortex for $CR \geq 20$ was found to occur at a constant value of a dimensionless normal stress ratio, proposed by Rothstein and McKinley (2001), $\mathcal{N} \approx 0.055$.

7. References

Aboubacar, M., Matallah, H. and Webster, M.F., 2002, "Highly elastic solutions for Oldroyd-B and Phan-Thien/Tanner fluids with a Finite Volume/Element Method: planar contraction flows", J. Non-Newtonian Fluid Mech., Vol.103, pp. 65-103.

Al Moatassime, H., Esselaoui, D., Hakim, A. and Raghay, S., 2001, "Finite volume multigrid method of the planar contraction flow of a viscoelastic fluid", Int. J. Numer. Meth. Fluids, Vol.36, pp. 885-902.

Alves, M.A., Pinho, F.T. and Oliveira, P.J., 2000, "Effect of a high-resolution differencing scheme on finite-volume predictions of viscoelastic flows", J. Non-Newtonian Fluid Mech., Vol.93, pp. 287-314.

Alves, M.A., Pinho, F.T. and Oliveira, P.J., 2001, "The flow of viscoelastic fluids past a cylinder: finite-volume high-resolution methods", J. Non-Newtonian Fluid Mech., Vol.97, pp. 207-232.

Alves, M.A., Oliveira, P.J. and Pinho, F.T., 2003a, "A convergent and universally bounded interpolation scheme for the treatment of advection", Int. J. Numer. Meth. Fluids, Vol.41, pp. 47-75.

Alves, M.A., Oliveira, P.J. and Pinho, F.T., 2003b, "Benchmark solutions for the flow of Oldroyd-B and PTT fluids in planar contractions", J. Non-Newtonian Fluid Mech., Vol.110, pp. 45-75.

Alves, M.A., Oliveira, P.J. and Pinho, F.T., 2003c, "Numerical simulation of viscoelastic contraction flows", Computational Fluid and Solid Mechanics 2003, Ed. Bathe, K.J., Elsevier, Amsterdam., Vol.2, pp. 826-829.

Alves, M.A., Oliveira, P.J. and Pinho, F.T., 2004, "On the effect of contraction ratio in viscoelastic flow through abrupt contractions", J. Non-Newtonian Fluid Mech., Accepted.

Baaijens, F.P.T., 1998, "An iterative solver for the DEVSS/DG method with application to smooth and non-smooth flows of the upper convected Maxwell fluid", J. Non-Newtonian Fluid Mech., Vol.75, pp. 119-138.

Coates, P.J., Armstrong, R.C. and Brown, R.A., 1992, "Calculation of steady-state viscoelastic flow through axisymetric contractions with the EEME formulation", J. Non-Newtonian Fluid Mech., Vol.42, pp. 141-188.

Evans, R.E. and Walters, K., 1986, "Flow characteristics associated with abrupt changes in geometry in the case of highly elastic liquids", J. Non-Newtonian Fluid Mech., Vol.20, pp. 11-29.

Hassager, O., 1988, "Working group on numerical techniques. Fifth international workshop on numerical methods in non-Newtonian flows, Lake Arrowhead, USA", J. Non-Newtonian Fluid Mech., Vol.29, pp. 2-5.

Matallah, H., Townsend, P. and Webster, M.F., 1998, "Recovery and stress-splitting schemes for viscoelastic flows", J. Non-Newtonian Fluid Mech., Vol.75, pp. 139-166.

McKinley, G.H., Raiford, W.P., Brown, R.A. and Armstrong, R.C., 1991, "Nonlinear dynamics of viscoelastic flow in axisymmetric abrupt contractions", J. Fluid Mech., Vol.223, pp. 411-456.

Meng, S., Li, X.K. and Evans, G., 2002, "Numerical Simulation of Oldroyd-B Fluid in a Contraction Channel", Journal of Supercomputing, Vol.22, pp. 29-43.

Nigen, S. and Walters, K., 2002, "Viscoelastic contraction flows: comparison of axisymmetric and planar configurations", J. Non-Newtonian Fluid Mech., Vol.102, pp. 343-359.

Oliveira, P.J., 2001, "On the numerical implementation of nonlinear viscoelastic models in a finite-volume method", Numer. Heat Transfer B, Vol.40, pp. 283-301.

Oliveira, P.J., Pinho, F.T. and Pinto, G.A., 1998, "Numerical simulation of non-linear elastic flows with a general collocated finite-volume method", J. Non-Newtonian Fluid Mech., Vol.79, pp. 1-43.

Oliveira, P.J. and Pinho, F.T., 1999, "Numerical procedure for the computation of fluid flow with arbitrary stress-strain relationships", Numer. Heat Transfer B, Vol.35, pp. 295-315.

Owens, R.G. and Phillips, T.N., 2002, "Computational Rheology", Imperial College Press, London.

Phan-Thien, N. and Tanner, R.I., 1977, "A new constitutive equation derived from network theory", J. Non-Newtonian Fluid Mech., Vol.2, pp. 353-365.

Phillips, T.N. and Williams, A.J., 1999, "Viscoelastic flow through a planar contraction using a semi-Lagrangian finite volume method", J. Non-Newtonian Fluid Mech., Vol.87, pp. 215-246.

Phillips, T.N. and Williams, A.J., 2002, "Comparison of creeping and inertial flow of an Oldroyd B fluid through planar and axisymmetric contractions", J. Non-Newtonian Fluid Mech., Vol.108, pp. 25-47.

Rothstein, J.P. and McKinley, G.H., 2001, "The axisymmetric contraction-expansion: the role of extensional rheology on vortex growth dynamics and the enhanced pressure drop", J. Non-Newtonian Fluid Mech., Vol.98, pp. 33-63.

Sasmal, G.P. (1995), "A Finite-Volume Approach for Calculation of Viscoelastic Flow- through an Abrupt Axisymmetrical Contraction", J. Non-Newtonian Fluid Mech., Vol.56, pp. 15-47.

Sato, T. and Richardson, S.M., 1994, "Explicit numerical simulation of time-dependent viscoelastic flow problems by a finite element/finite volume method", J. Non-Newtonian Fluid Mech., Vol.51, pp. 249-275.

Yoo, J.Y. and Na, Y., 1991, "A numerical study of the planar contraction flow of viscoelastic fluids using the SIMPLER algorithm", J. Non-Newtonian Fluid Mech., Vol.39, pp. 89-106.

Wachs, A. and Clermont, J.R., 2000, "Non-isothermal viscoelastic flow computations in an axisymmetric contraction at high Weissenberg numbers by a finite volume method", J. Non-Newtonian Fluid Mech., Vol.95, pp. 147-184.

8. Copyright Notice

The authors are the only responsible for the printed material included in this paper.